Quality-preserved Ambient Noise Imaging in Distributed Sensor Networks with Limited Bandwidth

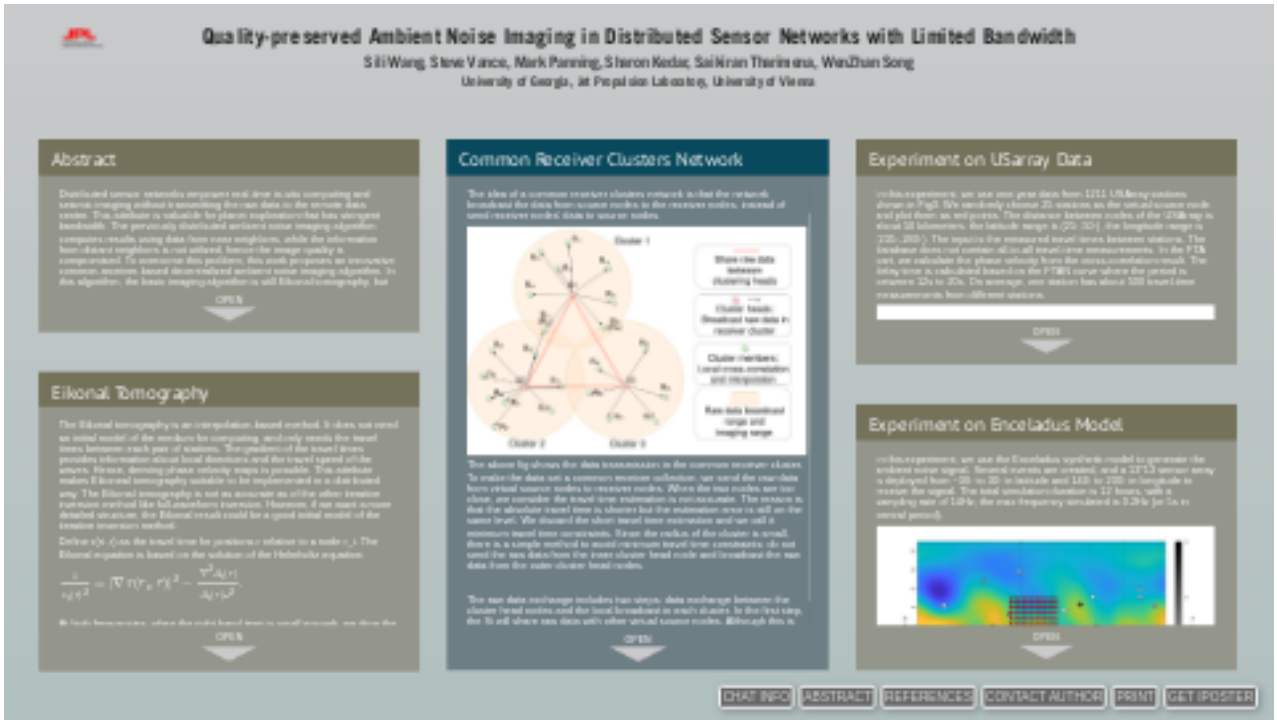

Sili Wang, Steve Vance, Mark Panning, Sharon Kedar, Saikiran Tharimena, WenZhan Song

University of Georgia, Jet Propulsion Laboratory, University of Vienna

PRESENTED AT:

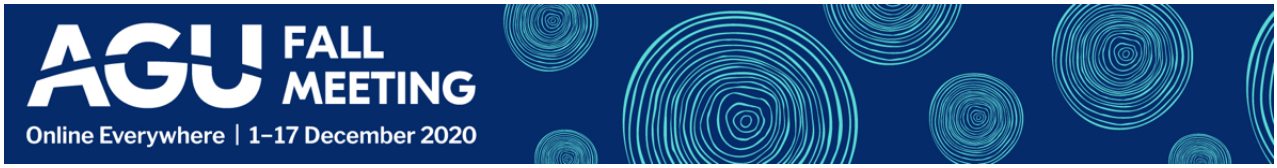

ABSTRACT

Distributed sensor networks empower real-time in-situ computing and seismic imaging without transmitting the raw data to the remote data center. This attribute is valuable for planet exploration that has stringent bandwidth. The previously distributed ambient noise imaging algorithm computes results using data from near neighbors, while the information from distant neighbors is not utilized, hence the image quality is compromised. To overcome this problem, this work proposes an innovative common-receiver-based decentralized ambient noise imaging algorithm. In this algorithm, the basic imaging algorithm is still Eikonal tomography, but the distant neighbors are also used to computing the seismic image so that the quality of the output image can be preserved. An in-situ computing and clustering algorithm is created to optimize the data transition and computation while meeting the bandwidth constraints. The experiments were performed on both synthetic data from Enceladus and real data from the USArray archives. The new algorithm generates higher-resolution images under the same bandwidth constraints, comparing to previous algorithms, and the quality of the output image is satisfactorily preserved. The communication cost reduction over the raw data collection is in several orders of magnitude (e.g., 1: 1600). It meets the desired bandwidth constraint in planetary exploration applications.

EIKONAL TOMOGRAPHY

The Eikonal tomography is an interpolation-based method. It does not need an initial model of the medium for computing, and only needs the travel times between each pair of stations. The gradient of the travel times provides information about local directions and the travel speed of the waves. Hence, deriving phase velocity maps is possible. This attribute makes Eikoneal tomography suitable to be implemented in a distributed way. The Eikonal tomography is not as accurate as of the other iterative inversion method like full-waveform inversion. However, if we want a more detailed structure, the Eikonal result could be a good initial model of the iterative inversion method.

Define τ(ri ,r) as the travel time for positions r relative to a node r_i. The Eikonal equation is based on the solution of the Helmholtz equation:

$$\frac{1}{c_i(r)^2} = |\nabla\tau(r_i, r)|^2 - \frac{\nabla^2 A_i(r)}{A_i(r)\omega^2}.$$

At high frequencies, when the right-hand term is small enough, we drop the second term on the right-hand side of the equation, we can get:

$$\frac{\hat{k}_i}{c_i(r)} \cong \nabla\tau(r_i, r),$$

where, c_i is the phase velocity for the event i at position r. k_i is the unit wave number vector for the event i at position r. The gradient is computed relative to the field vector r. It is clear that the slowness only depends on the local gradient on r.

In the isotropic model, to reduce the errors, a mean slowness S_0 and standard deviation are calculated to obtain the isotropic phase speed, following:

$$S_0 = \frac{1}{n}\sum_{i=1}^{n} S_i,$$

$$\sigma_{S_0} = \frac{1}{n(n-1)}\sum_{i=1}^{n}(S_i - S_0)^2,$$

where n is the stacking number. If we have enough stacking numbers, we can use the elliptical-anisotropic wave equation to measure the anisotropic phase wave velocity. S_i denotes the distribution of slowness measurements. The isotropic phase speed c_0, and its uncertainty are calculated as:

$$c_0 = \frac{1}{S_0}$$

$$\sigma_{c_0} = \frac{1}{S_0^2}\sigma_{S_0}.$$

COMMON RECEIVER CLUSTERS NETWORK

The idea of a common receiver clusters network is that the network broadcast the data from source nodes to the receiver nodes, instead of send receiver nodes' data to source nodes.

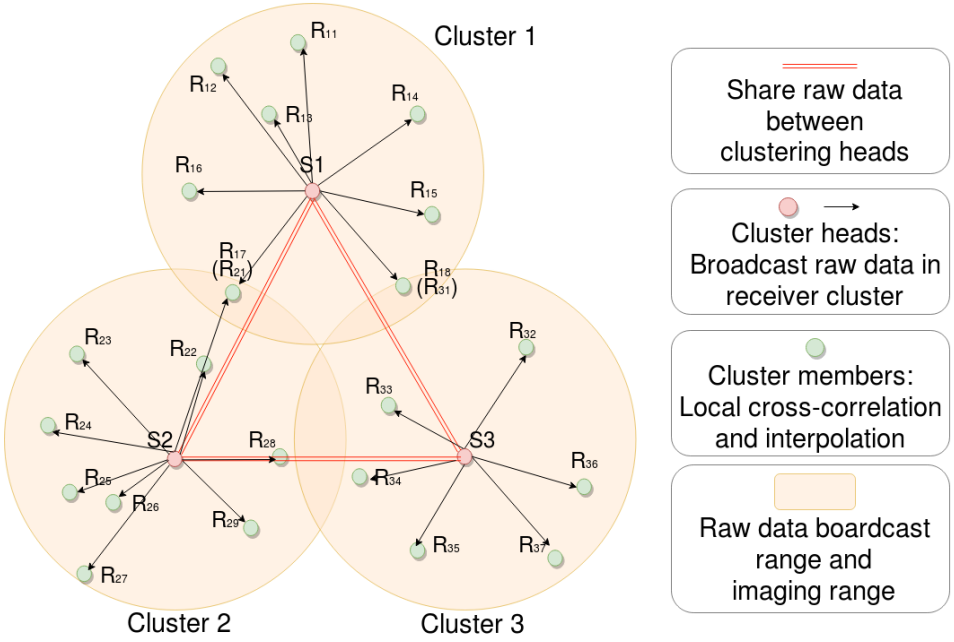

The above fig shows the data transmission in the common receiver cluster. To make the data set a common receiver collection, we send the raw data from virtual source nodes to receiver nodes. When the two nodes are too close, we consider the travel time estimation is not accurate. The reason is that the absolute travel time is shorter but the estimation error is still on the same level. We discard the short travel time estimation and we call it minimum travel time constraints. Since the radius of the cluster is small, there is a simple method to avoid minimum travel time constraints: do not send the raw data from the inner cluster head node and broadcast the raw data from the outer cluster head nodes.

The raw data exchange includes two steps: data exchange between the cluster head nodes and the local broadcast in each cluster. In the first step, the Si will share raw data with other virtual source nodes. Although this is long-distance data transmission, transmission only occurs on the backbone, and only the raw data originally from the virtual source node will be transmitted. After this step, all the virtual source nodes have a data set that contains the raw data from all virtual source nodes. The second step is that the virtual source nodes act as the cluster heads and broadcast the raw data package except its data. We do this because the receiver cluster is small and usually its cluster head does not meet the minimum travel time constraints. Finally, gathered on each receiver node, the data received by Rij should be:

$$
\begin{aligned}
&D_{recv}(R_{ij}) \\
&= D_{sent}(S_i) = D_{recv}(S_i) \\
&= D_{raw}(S_1, S_2, \ldots, S_{i-1}, S_{i+1}, \ldots).
\end{aligned}
$$

The workflow of Eikonal tomography in a common receiver sensor network is:

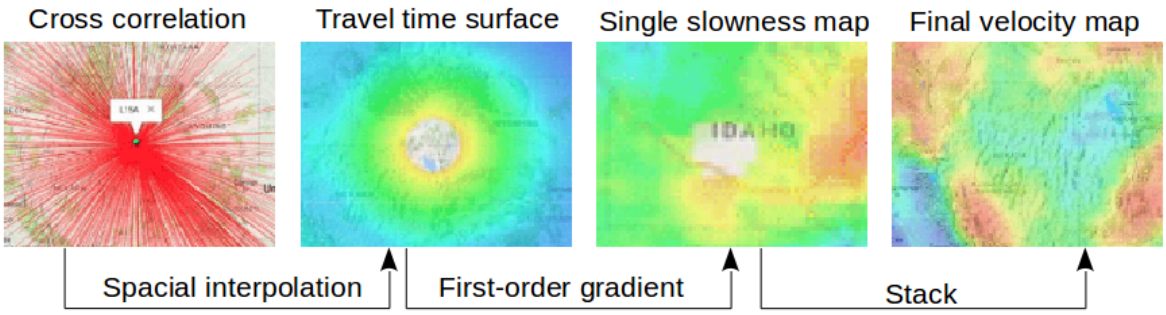
Cross correlation
Travel time surface
Single slowness map
Final velocity map
Spacial interpolation
First-order gradient
Stack

EXPERIMENT ON USARRAY DATA

In this experiment, we use one-year data from 1211 USArray stations shown in Fig3. We randomly choose 25 stations as the virtual source node and plot them as red points. The distance between nodes of the USArray is about 50 kilometers. the latitude range is (25◦,50◦), the longitude range is (235◦,280◦). The input is the measured travel times between stations. The database does not contain all-to-all travel-time measurements. In the FTA part, we calculate the phase velocity from the cross-correlation result. The delay time is calculated based on the FTAN curve where the period is between 12s to 20s. On average, one station has about 500 travel-time measurements from different stations.

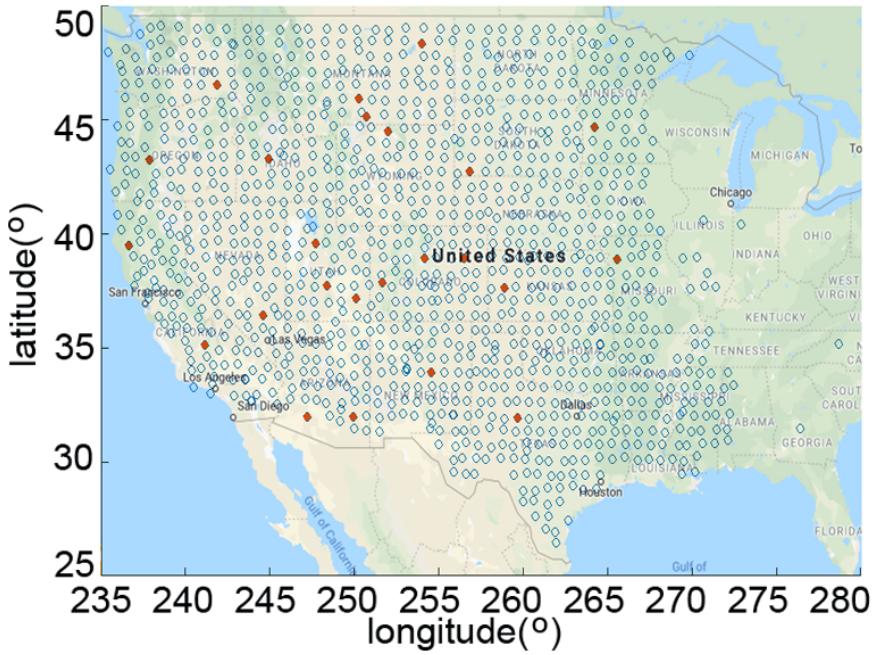

Fig4. (b) and (c) show the CS-TomoEK and CR-TomoEK results, respectively. Both of them use the same color map as a centralized result. From the figures, we can see that both the CS-TomoEK result and CR-TomoEK result reveal the basic structure of the velocity. However, the CS-TomoEK result has more small spurious structures that do not occur in the centralized result. The velocity range is also larger than the other two methods. The CR-TomoEK result is closer to the centralized result. In the high-velocity area, the CR-TomoEK result is very close to the centralized result; in the low-velocity area, the CR-TomoEK result has a lower velocity than the centralized result, but its velocity structure is similar to the centralized one. Also, the detail in the CS-TomoEK result is hard to explain by the geology information, it is the random variation. The CR-TomoEK result fits with the geology better with fewer abnormal structures. The results certify that using a common receiver-based algorithm can improve the quality of the output image.

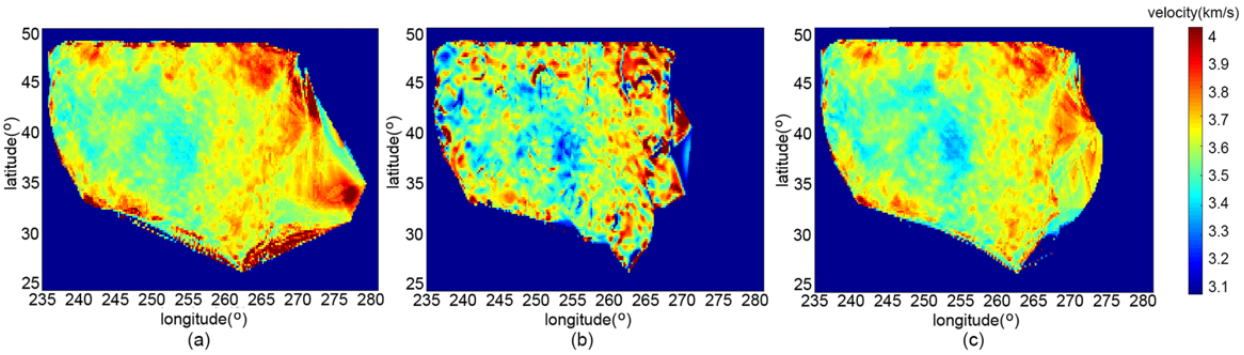
velocity(km/s)
4
3.9
3.8
3.7
3.6
3.5
3.4
3.3
3.2
3.1
latitude(°)
longitude(°)
(a)
(b)
(c)

EXPERIMENT ON ENCELADUS MODEL

In this experiment, we use the Enceladus synthetic model to generate the ambient noise signal. Several events are created, and a 13*13 sensor array is deployed from −30◦ to 30◦ in latitude and 140◦ to 200◦ in longitude to receive the signal. The total simulation duration is 12 hours, with a sampling rate of 14Hz, the max frequency simulated is 0.2Hz (or 5s in central period).

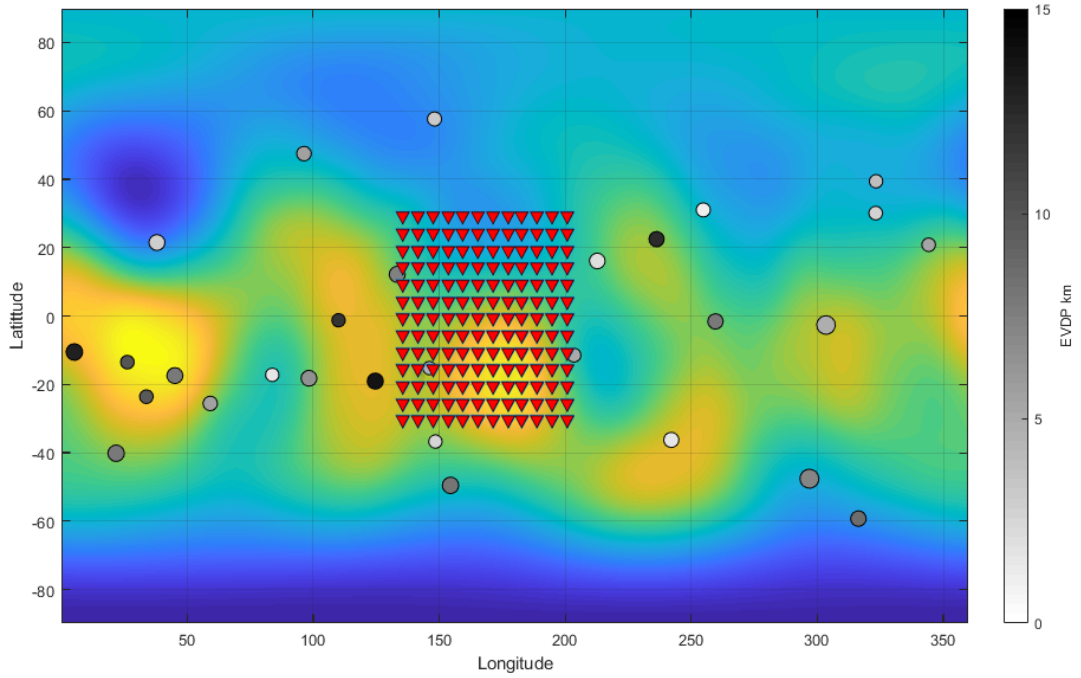

Fig. 6 shows the partial maps from four different sink nodes. On the partial map, we discard the value near the sink nodes because the delay time from the short distance pair has lower accuracy. This explains the hole that occurs on the partial maps in Fig. 6. Also, we can limit the transmission range to save communication traffic at the cost of the loss of the imaging range. As we can see, these maps have significant errors because they are just a partial view of the subsurface. We assume that the medium is isotropic, but it could also result in some error.

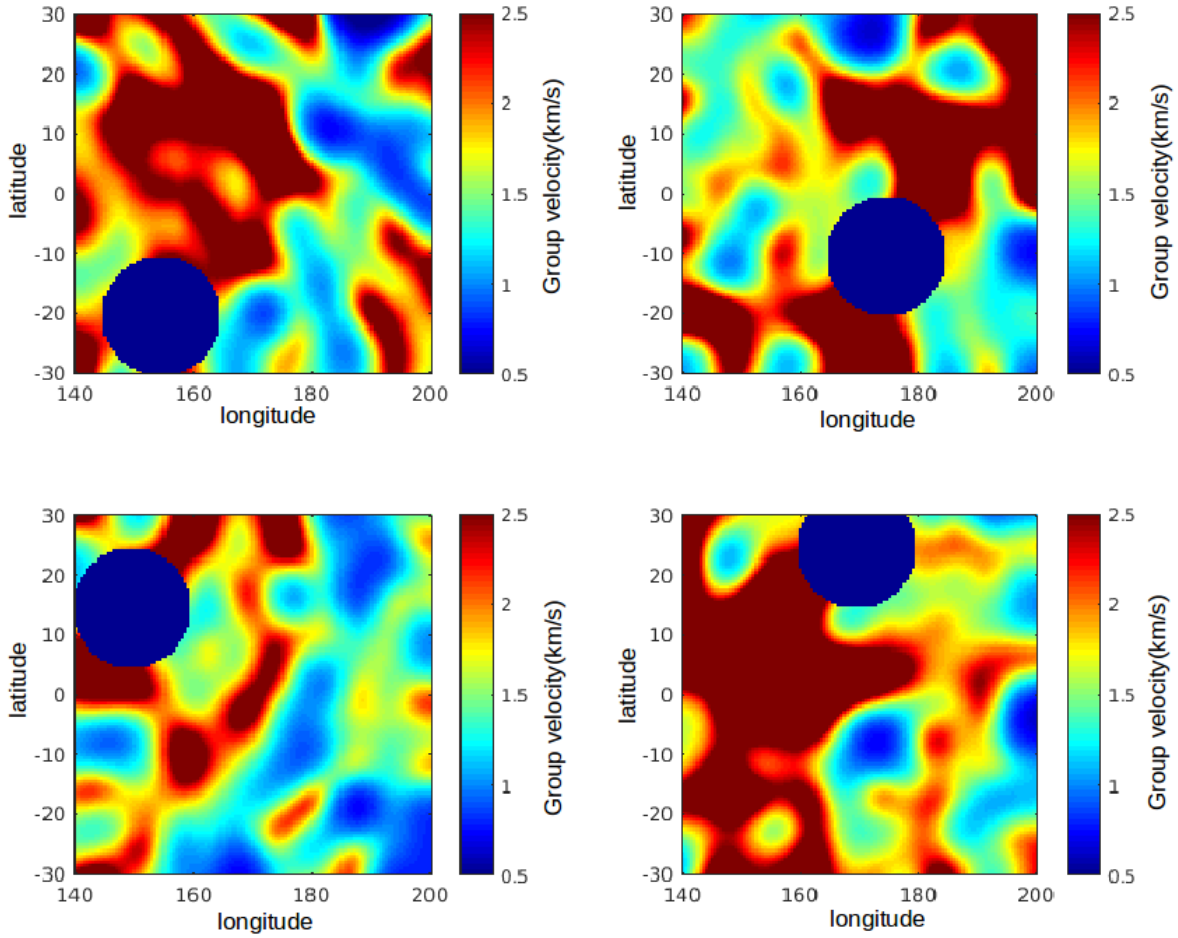

The final map is the stack result of the partial maps. The sink nodes will link to each other to share their partial map and update their final map periodically. Fig. 7 shows the final result we have in this experiment.

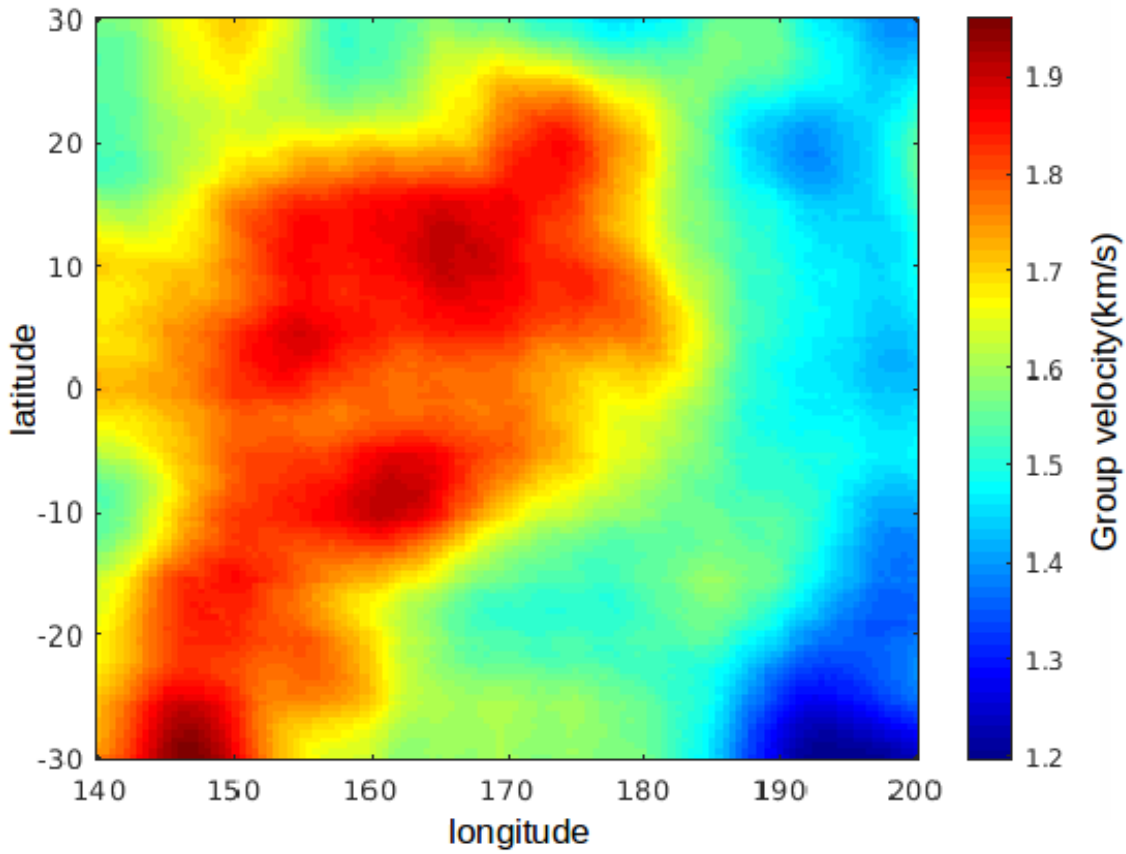
30
20
10
0
-10
-20
-30
latitude
140
150
160
170
180
190
200
longitude
1.9
1.8
1.7
1.6
1.5
1.4
1.3
1.2
Group velocity(km/s)

ABSTRACT

Distributed sensor networks empower real-time in-situ computing and seismic imaging without transmitting the raw data to the remote data center. This attribute is valuable for planet exploration that has stringent bandwidth. The previously distributed ambient noise imaging algorithm computes results using data from near neighbors, while the information from distant neighbors is not utilized, hence the image quality is compromised. To overcome this problem, this work proposes an innovative common-receiver-based decentralized ambient noise imaging algorithm. In this algorithm, the basic imaging algorithm is still Eikonal tomography, but the distant neighbors are also used to computing the seismic image so that the quality of the output image can be preserved. An in-situ computing and clustering algorithm is created to optimize the data transition and computation while meeting the bandwidth constrains. The experiments were performed on both synthetic data from Enceladus and real data from the USArray archives. The new algorithm generates higher-resolution images under the same bandwidth constraints, comparing to previous algorithms, and the quality of the output image is satisfactorily preserved. The communication cost reduction over the raw data collection is in several orders of magnitude (e.g., 1: 1600). It meets the desired bandwidth constraint in planetary exploration applications.

REFERENCES

S. Wang, F. Li, M. Panning, S. Tharimena, S. Vance and W. Song, "Ambient Noise Tomography With Common Receiver Clusters in Distributed Sensor Networks," in IEEE Transactions on Signal and Information Processing over Networks, vol. 6, pp. 656-666, 2020, doi: 10.1109/TSIPN.2020.3019328.

M. Valero, F. Li, S. Wang, F. Lin and W. Song, "Real-Time Cooperative Analytics for Ambient Noise Tomography in Sensor Networks," in IEEE Transactions on Signal and Information Processing over Networks, vol. 5, no. 2, pp. 375-389, June 2019, doi: 10.1109/TSIPN.2018.2876751.